BIOCHEMISTRY
including biophysical chemistry & molecular biology

Article

pubs.acs.org/biochemistry

Dissection of Porphyrin-Induced Conformational Dynamics in the Heme Biosynthesis Enzyme Ferrochelatase

Awuri P. Asuru, Mier An, and Laura S. Busenlehner*

Department of Chemistry, The University of Alabama, Tuscaloosa, Alabama 35487, United States

Supporting Information

ABSTRACT: Human ferrochelatase (EC 4.99.1.1) catalyzes the insertion ferrous iron into protoporphyrin IX as the last step in heme biosynthesis, an essential process to most organisms given the vast intracellular functions of heme. Even with multiple ferrochelatase structures available, the exact mechanism for iron insertion into porphyrin is still a matter for debate. It is clear, however, that conformational dynamics are important for porphyrin substrate binding, initial chelation of iron, insertion of iron into the macrocycle, and release of protoheme IX. In this work we characterize conformational and dynamic changes in ferrochelatase associated with porphyrin binding using the substrate mesoporphyrin (MPIX) and backbone amide hydrogen/deuterium exchange mass spectrometry (HDX-MS). In general, regions surrounding the active site become more ordered from direct or indirect interactions with the porphyrin. Our results indicate that the lower lip of the active site mouth is preorganized for efficient porphyrin binding, with little changes in backbone dynamics. The upper lip region has the most significant change in HDX behavior as it closes the active site. This movement excludes solvent from the porphyrin pocket, but leads to increased solvent access in other areas. A water lined path to the active site was observed, which may be the elusive iron channel with final insertion via the M76/R164/Y165 side of the porphyrin. These results provide a rigorous view of the ferrochelatase mechanism through the inclusion of dynamic information, reveal new structural areas for functional investigation, and offer new insight into a potential iron channel to the active site.

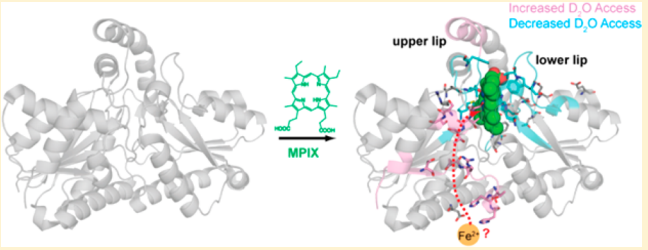

There is increasing evidence that protein dynamics are critical components to enzyme catalyzed reaction mechanisms.[1,2] The information gleaned from three-dimensional structures of enzymes has led to a revolution with regard to specific protein conformations associated with binding substrates, substrate analogues, transition state analogues, and products. However, the crystallographic structures of enzymes often do not reveal the sometimes slight, yet crucial, dynamic changes required for enzymatic processes. A rigorous measurement of protein dynamics is clearly needed to fully understand how localized motions in enzymes correlate with specific catalytic steps.[3] This information is valuable for designing therapeutic compounds that regulate the activity of key enzymes involved in disease, as well.[4] Amide hydrogen/deuterium exchange mass spectrometry (HDX-MS) provides a novel approach to define the role dynamics plays in enzyme-catalyzed reactions. The exchange rate of backbone amide hydrogens for deuterons is related to protein secondary structure, solvent accessibility, and backbone flexibility.[1] This makes amide hydrogens excellent reporters of protein structure and dynamics. It is especially useful for identifying functional changes in conformation when comparing two protein states (e.g., free enzyme vs substrate-bound enzyme). Thus, it is emerging as an attractive alternative or companion to other structural techniques due to the exceptional capability of examining both dynamic and structural components.

In this work, we report the structural and dynamic changes related to substrate binding for an important enzyme in heme biosynthesis, human ferrochelatase (E.C. 4.99.1.1). Ferrochelatase, the most extensively studied enzyme in the chelatase subclass, catalyzes the last step in heme biosynthesis, the insertion of ferrous iron (Fe^{2+}) in protoporphyrin IX (PPIX) to form protoheme IX.[5] The disease erythropoietic protophorphyria (EPP), where the PPIX intermediate accumulates in red blood cells and causes painful light sensitivity, is caused by characterized mutations in the FECH gene;[6,7] therefore, understanding the structure and mechanism of ferrochelatase is imperative for the development of treatments. Human ferrochelatase is an 84 kDa homodimer associated with the inner mitochondrial membrane, where the hydrophobic active site "mouth" is directed toward the membrane layer and flanked by two stretches of residues called the upper and lower "lips".[8] The upper lips also serve as insertion points into the membrane.[9] There are crystal structures of ferrochelatases from several organisms including *Bacillus subtilis*, *Bacillus anthracis*, *Saccharomyces cerevisiae*, and *Homo sapiens*.[8,10,11] This includes numerous structures with different metal ions,

Received: May 29, 2012
Revised: August 14, 2012
Published: August 16, 2012

substrates, products, and inhibitors, as well as site-directed mutants.[10,12−17]

The ferrochelatase catalytic cycle includes PPIX substrate binding, Fe^{2+} binding and desolvation, deprotonation of two PPIX pyrrole nitrogens, distortion of the PPIX macrocycle prior to Fe^{2+} insertion, and last, product release.[18] From structural analysis and other biochemical studies, it is apparent that ferrochelatase must undergo conformational changes in order to carry out these specific catalytic steps. However, sometimes these subtle changes in solution may not be easily detected in crystallographic structures. If these changes in dynamics can be identified, it would provide additional mechanistic information about how ferrochelatase inserts iron into PPIX. Knowledge of the ferrochelatase mechanism from a structural dynamics viewpoint is quite relevant for structure−activity based design of therapeutic compounds to regulate its activity as a treatment for EPP.

There are several crystal structures of human ferrochelatase with some form of porphyrin bound in the active site. The PPIX-bound structure of E343K ferrochelatase by Medlock et al.[20] indicates that the active site "mouth" closes around the substrate, resulting in the reorientation of key catalytic residues and changes in hydrogen bonding within the PPIX binding pocket.[12,20] Structures with heme and metalated porphyrins reveal that an unusual π-helix controls product release through winding and unwinding.[13,20] Thus, ferrochelatase undergoes changes in structure during the catalytic cycle and that control of dynamics may be important for distortion of the porphyrin macrocycle for iron insertion, chelation of iron, and release of heme.

There is still substantial debate as to how iron is acquired and inserted into PPIX in human ferrochelatase and its homologues. To address this gap in knowledge, prior HDX-MS was used to map conformational changes that occur when the cosubstrate Fe^{2+} binds to ferrochelatase in the absence of porphyrin substrate.[19] Those studies suggested that an iron-channel may exist from the mitochondrial matrix surface of the enzyme to the active site and supported a mechanism where the terminal iron acceptors before insertion are at or near R164 and Y165 on one face of the PPIX macrocycle. To gain a more complete picture of dynamic contributions to ferrochelatase catalysis, the changes in structure and dynamics critical for porphyrin substrate binding must also be defined. If PPIX binding signals iron uptake, then by comparison we can identify regions of ferrochelatase that are responsive only to porphyrin, only to iron, and to both substrates. The regions that have overlapping conformational changes are likely to be involved in the catalytic mechanism.

The research presented here uses HDX-MS to localize these important structural changes upon binding the substrate analogue mesoporphyrin IX (MPIX), which is structurally similar to PPIX (Chart 1). MPIX and is commonly used in enzyme activity assays because it is more stable and soluble than its native substrate PPIX.[16,21] HDX-MS provides insight into the coupling of PPIX binding with Fe^{2+} uptake, thus providing a more detailed structural view of the ferrochelatase mechanism, which is still debated. A potential water-accessible pathway from the surface of the protein to the active site was observed upon MPIX binding that could serve as an iron substrate channel, and thus HDX-MS has provided needed information about this key enzymatic process and opened new avenues for biochemical investigation.

Chart 1

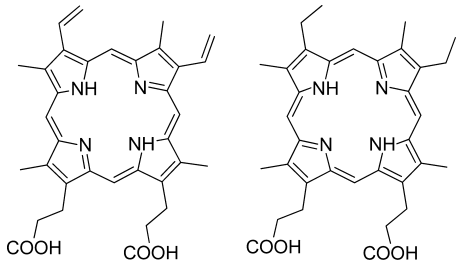

MATERIALS AND METHODS

Materials. ACS grade HEPES, HPLC grade water, and HPLC grade acetonitrile were obtained from EMD Chemicals (Billerica, MA), CHAPS from Applichem (St. Louis, MO), mesoporphyrin IX from Frontier (Logan, UT), deuterium oxide 99.99% at. D from Acros Organics (Geel, Belgium), porcine pepsin (3200−4500 units/mg) from Sigma-Aldrich (St. Louis, MO), HPLC grade 2-propanol from Honeywell (Morristown, NJ), Ni-NTA Superflow affinity resin from 5 Prime (Gaithersburg, MD), Circlegrow medium from Bio101 (Vista, CA), and HB101 competent cells from Promega (Madison, WI). A Bruker HCTultra Discovery mass spectrometer (Billerica, MA) was used with an Agilent 1100 liquid chromatography system (Santa Clara, CA).

Ferrochelatase Expression and Purification. *Escherichia coli* HB101 cells were transformed with pHisTF20E provided by Dr. Harry Dailey (University of Georgia) and plated on Luria−Bertani agar with 100 μg/mL ampicillin.[9] A single colony was used to inoculate 2 L of Circlegrow medium that was supplemented with 50 μg/mL carbenicillin. Protein expression and purification are as described.[19] Purified ferrochelatase was dialyzed extensively against 4 L of chelexed 25 mM HEPES (pH 7.4), 100 mM NaCl, 20 mM β-mercaptoethanol, and 0.1% CHAPS at 4 °C in nitric acid washed glassware. The concentration of ferrochelatase was estimated at 278 nm (ε_{278} = 46 910 M^{-1} cm^{-1}) and the percentage of bound [2Fe-2S] cluster was estimated by the absorbance at 330 nm (ε_{330} = 12 000 M^{-1} cm^{-1}).[9] The iron content of purified free-ferrochelatase was measured by atomic absorption spectroscopy and found to be 1.8 ± 0.1 mol iron per mol ferrochelatase, as expected if each monomer contains the [2Fe-2S] cluster. UV−visible spectroscopy also confirmed that the extensively dialyzed, purified ferrochelatase contained less than 5% of porphyrin in the active site, as determined by loss of the characteristic Soret band.[22] We refer to this preparation as the free-enzyme. Previously we reported that CHAPS-solubilized ferrochelatase in the presence of reducing agent with incubation under N_2, as in HDX samples, retained the [2Fe-2S] cluster and ∼95% activity over 2 h at 25 °C.[19]

Hydrogen/Deuterium Exchange. The peptides that result from a pepsin digest of ferrochelatase were reported in ref 19. The full peptide map has approximately 74% sequence coverage by the peptides used reproducibly for H/D exchange (Figure S1). A fresh 1 mM mesoporphyrin IX (MPIX) stock was prepared in 12 mM ammonium hydroxide and 1% CHAPS in chelexed ddiH_2O. Approximately 1.2 mol equiv of MPIX was added to 20 μM ferrochelatase pretreated with 40 μM EDTA (pH 8.0) to chelate any residual iron. Samples of MPIX-bound

dx.doi.org/10.1021/bi300704c | *Biochemistry* 2012, 51, 7116−7127

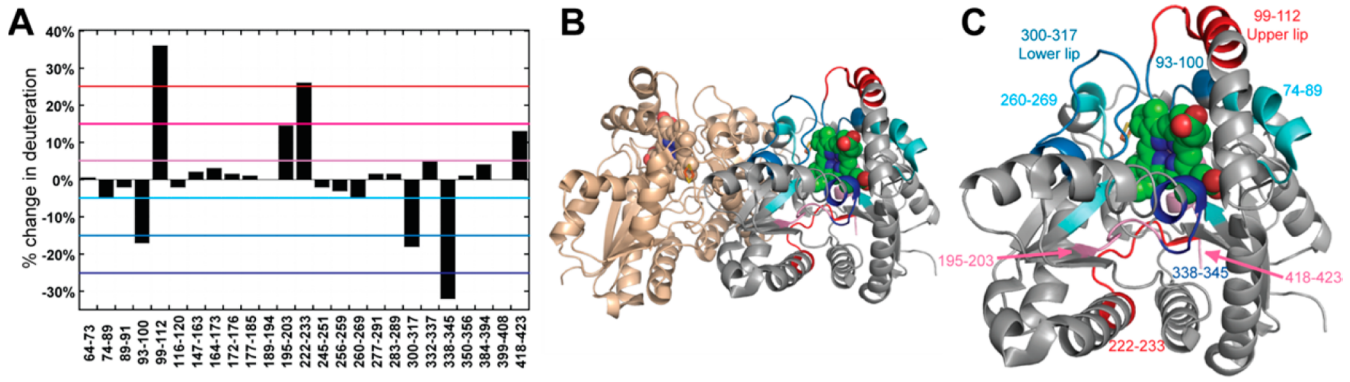

Figure 1. Difference in D_2O accessibility to free-ferrochelatase backbone amides when MPIX is bound. (A) The percentage of deuterium lost or gained after a 15 s incubation in D_2O was calculated for each pepsin-digested peptide. The cyan, light blue, and dark blue lines signify a greater than 5, 15, and 25% decrease in deuterium incorporation, respectively. The pink, magenta, and red lines signify a greater than 5, 15, and 25% increase in deuterium incorporation, respectively. The color coded peptides from (A) are plotted on (B) the PPIX-ferrochelatase dimeric structure derived from PBD 2QD1[20] and (C) one monomer subunit using PyMOL.[32]

ferrochelatase were aliquoted into thin-walled PCR tubes, wrapped in foil, and flash-frozen at −80 °C until HDX analysis.

Deuterium exchange was initiated by the addition of 45 μL of D_2O into 5 μL of ∼20 μM free or MPIX-ferrochelatase at 23 °C in a thin-walled PCR tube. The deuterium-protein samples were quickly purged with N_2 gas for the longer time points, incubated at 23 °C, and exchange was quenched at specific time points (15 s−2 h) by 50 μL of quench buffer [0.1 M potassium phosphate (pH 2.3) in H_2O; 0 °C]. The sample was immediately transferred to an ice bath. Porcine pepsin in 10 mM potassium phosphate, pH 7.0 was added to the sample (40 μg) and the digestion proceeded for 5 min. The peptide digests were separated by liquid chromatography on a 1 mm × 50 mm C18 reverse-phase column (Phenomenex, Torrence, CA) submerged in an ice water bath and the mass spectra were collected, as described.[19]

The chromatographic retention profiles for each identified peptide ion were extracted for all samples. The spectra within the elution peak were averaged to produce a composite spectrum for each peptide ion. The centroid (m_t) of the given composite isotope envelope was calculated by MagTran 1.0 beta 9 software[23] and also by Sierra Analytics software HDExaminer (http://www.massspec.com/HDExaminer.html) with equivalent results. For multiply charged peptide ions, the isotopic envelopes from each charge state were averaged when appropriate. The amount of deuterium incorporated at each time point was calculated using

$$D = N\left(\frac{m_t - m_{0\%}}{m_{100\%} - m_{0\%}}\right) \quad (1)$$

where $m_{0\%}$, m_t, and $m_{100\%}$ are the centroid values of the peptide in the non-deuterated, the partially deuterated at time t, and the fully deuterated control samples, respectively.[24] N is the total number of exchangeable peptide amide protons less one for the N-terminal amide proton and any proline residues. The amount of deuterium incorporated in each peptide was averaged from three independent kinetic runs and plotted as a function of time in minutes. The resulting progress curve for each peptide was fit using KaleidaGraph (Synergy Software) to single or double exponential equations as appropriate. All HDX-MS kinetic traces with fits are provided in Supporting Information available free of charge via the Internet at http://pubs.acs.org.

RESULTS

General Considerations. The kinetics of base catalyzed (OD^-) deuterium exchange at backbone amide protons is dependent on a variety of factors.[25,26] The first 15 s of a HDX time course provides a rough estimate of the relative solvent accessibility of backbone amides as it is related to the secondary and tertiary structure of the protein.[27,28] HDX is useful for localizing ligand binding interactions through protection of amide hydrogens in the ligand binding site.[29,30] The specific amides protected by the ligand are identified after pepsin digestion and MS through a decrease in deuterium incorporation as compared to the free protein. It should be noted that some large conformational changes outside a ligand binding site may bury previously exposed amides thereby also decreasing deuterium incorporation, so a full characterization of H/D exchange kinetics is required to help differentiate these possibilities. To determine the effect of substrate binding on ferrochelatase, we compared the relative solvent accessibility of the iron-free enzyme to the MPIX-bound form after 15 s incubation in D_2O. The changes in solvent accessibility with the cosubstrate Fe^{2+} have already been characterized.[19]

HDX Solvent Accessibility. A difference plot of the percent deuterium incorporation in MPIX-ferrochelatase backbone amides relative to free enzyme is shown in Figure 1A. The corresponding peptides are indicated on the structure of E343K ferrochelatase with PPIX bound,[20] to which the HDX results will be compared (Figure 1B,C). Considerable protection by MPIX from deuterium exchange is observed for peptide residues 93−100, 300−317, and 338−345, with minor protection for peptides 74−89 and 260−269. These regions surround the porphyrin binding site, as expected, with the greatest protection observed for peptide 338−345. This peptide resides at the beginning of the π-helix$_{13}$ and has residues within van der Waals distance to PPIX. Modest protection from deuterium exchange is shown for residues in the upper (93−100) and lower (300−317) lips of the porphyrin binding site. On the basis of the PPIX structure, the upper lip peptide 93−100 has several residues whose side chains are within 3.5 Å of the porphyrin. The lower lip peptide 300−317 is highly conserved and located in a loop opposite the porphyrin binding pocket as 93−100. Several residues within this peptide interact with PPIX in the crystal structure. Two peptides, 74−89 and 260−269, show minor decreases in solvent accessibility in

dx.doi.org/10.1021/bi300704c | Biochemistry 2012, 51, 7116−7127

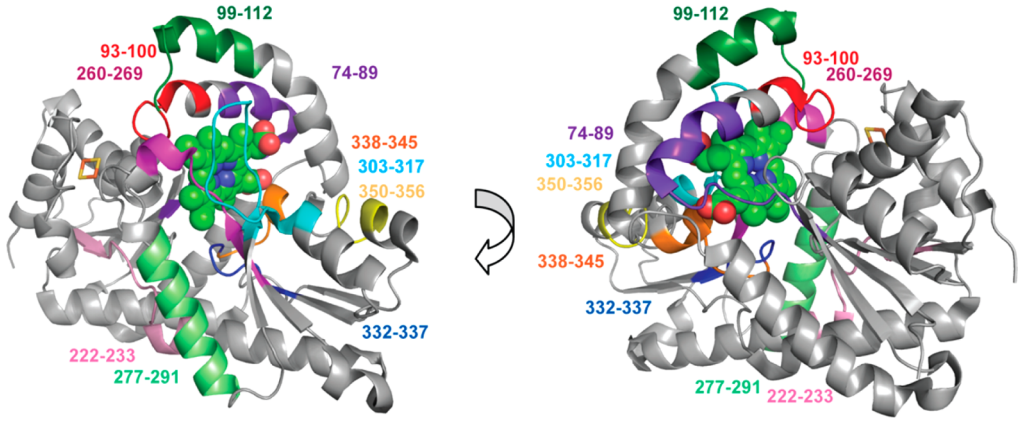

Figure 2. Ferrochelatase peptides with decreased backbone dynamics after binding MPIX. The peptides identified as having a decrease in one or more rate constant for exchange are mapped onto PPIX-ferrochelatase[20] and are colored as follows: 74−89 (purple), 93−100 (red), 99−112 (dark green), 222−233 (pink), 260−269 (magenta), 277−291 (light green), 303−317 (cyan), 332−337 (blue), 338−345 (orange), and 350−356 (yellow). PPIX is in green spheres and the [2Fe−S] cluster is in stick format. The structure on the right was rotated 180°. Figure created with PyMOL.[32]

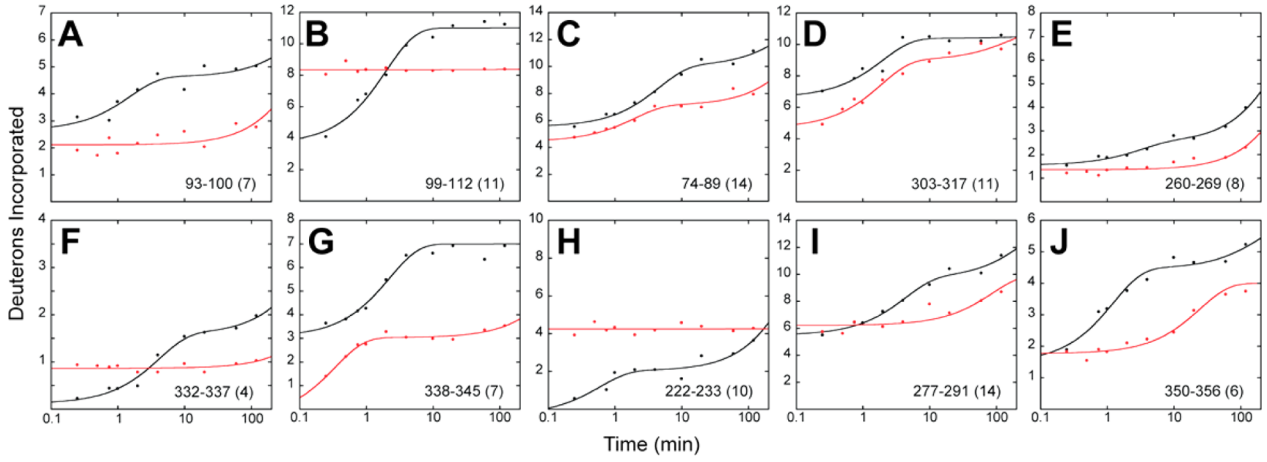

Figure 3. HDX-MS rate profiles for selected ferrochelatase peptides. Shown are the kinetic traces for the number of deuterons incorporated into peptides derived from free (black) and MPIX (red) ferrochelatase as a function of incubation time in D_2O. The data are an average of 2−3 sets and were fit to single or double exponential equations to obtain the rate constants for exchange (k_n) and the corresponding number of deuterons in each phase (D_n). The fitted parameters are given in Table 1. The numbers in parentheses are the total number of exchangeable amide protons for each peptide. (A) 93−100. (B) 99−112. (C) 74−89. (D) 303−317. (E) 260−269. (F) 332−337. (G) 338−345. (H) 222−233. (I) 277−291. (J) 350−356. The peptides are mapped on the monomeric structure in Figure 2.

MPIX-bound ferrochelatase. The region spanning residues 74−89 is N-terminal to the upper lip that has significant protection and contains two residues within interaction distance to PPIX. Peptide 260−263 is on the opposite face of the porphyrin and contains H263, a key residue in the binding site that has a role in the catalytic mechanism.[31] In summary, the areas protected by MPIX are within the immediate binding pocket.

There are also regions of ferrochelatase that display an increase in deuterium incorporation in the MPIX-bound form compared to the free enzyme (Figure 1A−C). This likely denotes a conformational change that exposes previously inaccessible amide protons to D_2O. The largest changes in solvent accessibility occur for peptides 99−112 and 222−233. Peptide residues 99−112 are in $helix_2$ above the porphyrin binding pocket.[20] As the major component to the upper lips, this region is thought to interact with the inner mitochondrial membrane layer. It immediately follows peptide 93−100 that showed significant solvent protection by MPIX. Peptide 99−112 is farther away from the active site compared to 93−100 and has no observed interactions with PPIX based on the structure. Peptide 222−233 is over 11 Å away from the substrate binding site. This region may initially bind iron at the protein surface.[8] Minor increases in D_2O access in the presence of MPIX is noted for peptides 195−203 and 418−423. Peptide 195−203 is close to the porphyrin site and may reside in an iron channel. The last area of increased solvent accessibility is at the C-terminus, peptide 418−423. It is unclear what role this region may play in binding substrate porphyrins. The region must be important since many mutations that cause EPP are located in the dimer interface.[6,7]

Dynamics of MPIX Binding. In general, substrate binding to an active site often results in decreased backbone dynamic motions and rates of deuterium incorporation as compared to the free enzyme.[33] This can be attributed to additional interactions with residue side chains that constrain backbone dynamics, but it can also be the result of increased hydrogen bonding within backbone amides themselves (i.e., changes in secondary structure).[34] For ferrochelatase we examined regions of the enzyme where the rate of deuterium incorporation into backbone amides was decreased upon MPIX binding,

dx.doi.org/10.1021/bi300704c | *Biochemistry* 2012, 51, 7116−7127

Table 1. HDX-MS Rate Constants and Amplitudes for Peptides from Figure 3[a]

peptide	pre-exchanged[b] "fast"	D_1	k_1 (min^{-1}) "intermediate"	D_2	k_2 (min^{-1})[c] "slow"
A: 93−100(7)					
free	~2.7	2.0 (±0.5)	0.7 (±0.3)	2.4 (±0.2)	≤1 × 10^4
MPIX	~2			4.9 (±0.1)	≤1 × 10^4
B: 99−112(11)					
free	~3.8	7.2 (±0.4)	0.50 (±0.06)		
MPIX	~8.1			2.85 (±0.09)	≤1 × 10^4
C: 74−89(14)					
free	~5.5	4.5 (±0.4)	0.22 (±0.05)	4.0 (±0.4)	2.3 (±0.9) × 10^3
MPIX	~4.4	2.7 (±0.4)	0.5 (±0.1)	6.9 (±0.3)	1.5 (±0.6) × 10^3
D: 303−317 (11)					
free	~6.8	4.2 (±0.5)	0.4 (±0.1)	~4	≤1 × 10^4
MPIX	~4.8	4.2 (±0.4)	0.5 (±0.1)	2.0 (±0.2)	6.1 (±0.3) × 10^3
E: 260−269 (8)					
free	~1.6	0.9 (±0.1)	0.32 (±0.09)	5.5 (±0.1)	2.5 (±0.4) × 10^3
MPIX	~1.4			6.64 (±0.06)	1.3 (±0.2) × 10^3
F: 332−337 (4)					
free	~0	1.5 (±0.1)	0.24 (±0.06)	2.4 (±0.1)	1.3 (±0.7) × 10^3
MPIX	~0.9			3.13 (±0.03)	≤1 × 10^4
G: 338−345 (7)					
free	~3.1	3.9 (±0.3)	0.45 (±0.08)		
MPIX	~2.8	3.4 (±0.6)	2.9 (±0.6)	3.97 (±0.07)	≤1 × 10^4
H: 222−233 (10)					
free	~0	2.3 (±0.9)	1.7 (±0.9)	7.9 (±0.2)	1.9 (±0.6) × 10^3
MPIX	~4.3			5.76 (±0.09)	≤1 × 10^4
I: 277−291(14)					
free	~5.5	4.2 (±0.4)	0.23 (±0.07)	4.3 (±0.4)	3 (±1) × 10^3
MPIX	~6.3			7.7 (±0.2)	0.01 (±0.3)
J: 350−356(6)					
free	~1.4	3.0 (±0.4)	0.81 (±0.09)	1.6 (±0.2)	5.0 (±0.2) × 10^3
MPIX	~1.8	2.23 (±0.08)	0.041 (±0.007)	~2	≤1 × 10^4

[a]Parameters obtained from fitting the H/D-exchange kinetics of ferrochelatase peptides with and without MPIX (Figure 3A−J) according to a single or double exponential expression. The number in parentheses is the total possible number of exchangeable amide hydrogens (N) for that peptide. The rates have been loosely grouped in to fast, intermediate, and slow exchange. [b]The amount of exchange before the first time point (15 s) is estimated from the fit parameters and is assigned a rate of exchange >4 min^{-1}. [c]The amount of deuterium in the slowest phase was determined $D_2 = N - D_1 - D_{pre\text{-}exchanged}$.

irrespective of solvent accessibility. This provides a more complete picture of the conformational changes associated with occupation of substrate in the active site. HDX-MS kinetic analysis identifies 10 peptides with decreased backbone dynamics in the MPIX bound state. The peptides are mapped to the PPIX-ferrochelatase structure (Figure 2) that will serve as the reference structure for HDX results.[20] Note that deuterium incorporation profiles that are unchanged with time could indicate that conformational changes upon addition of MPIX were too fast to be observed (i.e., k_{ex} > 4 min^{-1}) by this method, especially if there is significant deuterium incorporation before the first 15 s. Therefore, we cannot rule out that there are key conformation and dynamic changes to the catalytic mechanism that we cannot detect. Additionally, for some peptides, amide proton exchange did not increase over the 2 h incubation in D_2O. With additional incubation, it may be possible for those amides to eventually exchange. The slower conformational changes in ferrochelatase structure reported here should be taken as a reflection of the global folding/unfolding motions all proteins undergo as reflected by their thermodynamic stabilities.

Active Site Dynamics. The majority of peptides surround the porphyrin binding site, as expected. HDX rates for the two upper lip peptides, 93−100 and 99−112, are decreased two- and three-orders of magnitude, respectively (Figure 3A,B). Several amino acid side chains in peptide 93−100 are within interaction distance to the porphyrin. With the additional interactions constraining loop flexibility, the overall rate of deuterium incorporation into the backbone is also decreased. Although peptide 99−112 has no direct contact with porphyrin, it is likely that decreased dynamics are the result of its location in the upper lip. Other changes in dynamics faster than can be measured manually (k_{ex} > 4 min^{-1}) cannot be ruled out, especially with the flat progress curve.

Another peptide N-terminal to the upper lip, 74−89, has a slight decrease in exchange kinetics and a reduction in overall deuterium content upon MPIX binding (Figure 3C). This peptide contains an interaction with PPIX via M76 that could constrain dynamic motion.

The lower lip of the active site, comprised by peptide 303−317, does not show the same large reduction in HDX kinetics with MPIX that was observed for the upper lip peptides (Figure 3D). This peptide is an extended loop opposite the upper lip of the porphyrin binding site and residues V305 and W110 interact with PPIX.[20] Exchange rates are generally faster in unstructured loops compared to areas with hydrogen bonded secondary structure, so minor decreases in HDX kinetics even with interactions to PPIX are not unexpected.[1] Near the lower

dx.doi.org/10.1021/bi300704c | Biochemistry 2012, 51, 7116−7127

lip on the same face of the porphyrin is peptide 260−269 (Figure 3E). It has a 3-fold decrease in the rate of exchange when MPIX is bound, likely due to interactions between H263 and PPIX. H263 sits atop the pyrrole nitrogens and is much closer to the porphyrin ring than residues within peptide 303−317. There is little change in D_2O access to backbone amides, as well.

Dynamics beyond the Active Site. There are three peptides located outside the MPIX binding pocket with decreased rates of deuterium incorporation, indicating that binding transmits conformational changes to other areas that may be functionally important. Peptide 222−233 is one potential entry point for iron identified by previous H/D exchange experiments,[19] and a ferrochelatase crystal structure,[8] peptide 277−291 is in $helix_{11}$ at the dimerization interface, and peptide 350−356 is in the middle of the π-$helix_{13}$. The deuterium exchange rate for peptide 222−233 is too slow to be accurately measured (Figure 3H), while that of peptide 277−291 is decreased ∼2-fold in the presence of MPIX (Figure 3I). The decrease for residues 222−233 may indicate that the putative iron entrance pathway responds to MPIX in the active site to prepare for initial iron binding.[19] Again, changes in dynamics occurring faster than we can measure with the current technique are feasible. For peptide 277−291, it is possible that porphyrin binding causes a slight conformational change at the dimer interface (Figure 3I). Finally, peptide 350−356 shows a 16-fold decrease in the rate in the presence of MPIX (Figure 3J). This increased stability could be functionally significant for the ferrochelatase mechanism since helix unwinding is involved in product release.[13,20]

DISCUSSION

While vital structural information is gained from X-ray crystallography, a more complete view of protein function must include changes in dynamics and conformation. This is especially true for enzymes, where these properties are often related to catalytic efficiency.[2,4] Defining mobile and constrained regions can help dissect the individual steps in a catalytic cycle. For example, it is necessary to understand what regions are involved in substrate binding and how that affects areas near the active site. But in many cases it is the change in structure or dynamics outside the immediate vicinity of the active site than can yield additional information. These areas may not have an obvious structural connection to the active site and, as a result, can be overlooked by functional studies.

We used HDX-MS to define functional and structural regions of human ferrochelatase involved in binding mesoporphyrin IX, an analogue of the native substrate protoporphyrin IX.[16] These results are compared to those with the cosubstrate ferrous iron[19] to give insight into how these two binding events may be structurally linked. The role of active site dynamics toward the mechanism and the potential paths for iron binding and delivery to the bound porphyrin are discussed.

A global HDX-MS analysis with intact ferrochelatase was attempted to describe the overall change in deuterium incorporation when MPIX binds at the active site. Unfortunately, the large size (84 kDa) of ferrochelatase solubilized with CHAPS detergent and the highly hydrophobic substrate porphyrin severely suppressed ion signals making global HDX analysis difficult. To get a better feeling of global behavior, the number of amides exchanging in the fast, intermediate, and very slow phases were calculated from the kinetic fits to peptides spanning the ferrochelatase sequence. Of the peptides identified, MPIX binding results in 10 additional amides exchanging for deuterons in the fast time regime, a loss of 35 amides in the intermediate regime, and a gain of 24 in the slow regime (Table 2). This indicates that porphyrin substrate causes an overall increase in solvent accessibility, but it also stabilizes the global structure since the number of slow exchanging amides increases. Some of those amides most certainly were at the expense of intermediate exchanging protons, which reflect the local dynamic changes after substrate binding. The HDX results suggest that MPIX does not drastically change the overall secondary structural content but that protein dynamics could play a substantive role in catalysis.

Table 2. Global HDX Analysis of Characterized Ferrochelatase Peptides[a]

	number of exchanged amide protons (N = 194)		
	free	MPIX	difference
fast[b]	47.6	57.7	+ 10.1
intermediate[c]	104.5	69.2	−35.3
slow[d]	41.7	65.9	+24.2

[a]The number of exchanged protons for deuterons was obtained from fits to the H/D-exchange kinetics of ferrochelatase peptides with and without MPIX as found in Supporting Information. [b]Fast exchange, $k_{ex} > 4$ min^{-1}. [c]Intermediate exchange, 4 min^{-1} < k_{ex} > 1 × 10^{-4} min^{-1}. [d]Slow exchange, $k_{ex} < 1 \times 10^{-4}$ min^{-1}.

Porphyrin Binding Is Controlled by Reorientation of the Upper Lip. The most obvious changes in conformation identified by HDX-MS occur around the ferrochelatase active site, particularly around the upper lip. This is also observed in the crystal structures with and without PPIX.[20] The upper lip of the PPIX binding site mouth spans $helix_1$ to $helix_3$ (residues 90−130). The loop peptide 93−100 connects $helix_1$ to $helix_2$ and the adjacent peptide 99−112 is solely in $helix_2$ (Figure 2). While these two upper lip peptides are stably folded and dynamically constrained (Figure 3A,B), they have different solvent accessibilities when MPIX is present (Figure 1A). MPIX binding decreases the amount of deuterium incorporation for peptide 93−100, but increases for 99−112. This is likely due to interactions with PPIX for peptide 93−100 such as L98 and M99 that helps clamp the active site mouth around the porphyrin, decreasing the D_2O accessibility of those amides (Figure 4, red). In contrast, peptide 99−112 has higher solvent accessibility initially, but no additional deuterium is incorporated after that. While this decrease in exchange with MPIX indicates more stability toward the slower folding/unfolding states of ferrochelatase, it is also possible that the higher solvent accessibility for this peptide could reflect that MPIX increases the local dynamics that are faster than measurable by HDX-MS. Despite not directly interacting with the substrate, upper lip residues in $helix_2$ have a conformational response to MPIX. This is also discerned from the crystal structure alignments with and without PPIX[20] (Figure 4, dark green). Compared to Fe^{2+}-ferrochelatase, the rate profiles of peptides 93−100 and 99−112 in the presence of iron are virtually identical to the free-enzyme.[19] This indicates that the conformational response is exclusively due to porphyrin binding, which is likely communicated through residues 93−100.

Another upper lip peptide, 116−120 in $helix_3$ (Figure 4A, brown), is completely solvent inaccessible with very stable hydrogen bonding in free-, MPIX-, and Fe^{2+}-ferrochelatases over a 2 h HDX time course (Figure 4B), despite showing

dx.doi.org/10.1021/bi300704c | Biochemistry 2012, 51, 7116−7127

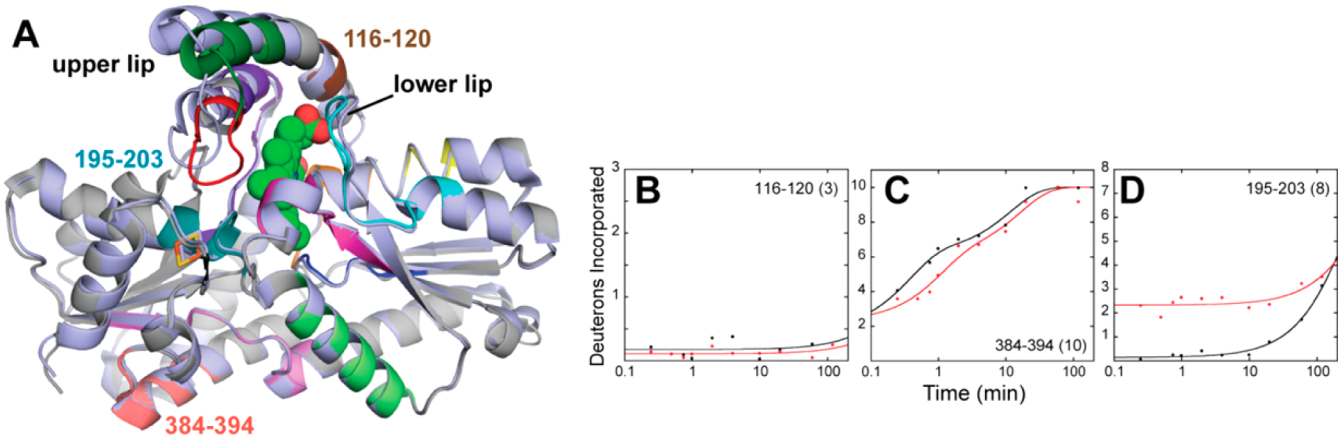

Figure 4. Structure overlay of free- and PPIX-ferrochelatase with key HDX peptides. (A) The backbones of free (PDB 2QD4; lavender) and PPIX (PDB 2QD1; gray with colors) ferrochelatase[20] were aligned with PyMOL.[32] 74–89 (purple), 93–100 (red), 99–112 (dark green), 116–120 (brown), 195–203 (dark teal), 222–233 (pink), 260–269 (magenta), 277–291 (light green), 303–317 (cyan), 332–337 (blue), 338–345 (orange), 350–356 (yellow), and 384–394 (salmon). PPIX is in green spheres. (B–D) HDX-MS rate profiles derived from free (black) and MPIX (red) ferrochelatase are shown for (B) 116–120, (C) 384–394, and (D) 195–203. The data were fit as in Figure 3 and reported in Table 3.

Table 3. HDX-MS Rate Constants and Amplitudes for Peptides from Figure 4[a]

peptide	pre-exchanged[b] "fast"	D_1	k_1 (min^{-1}) "intermediate"	D_2	k_2 (min^{-1})[c] "slow"
A: 116–120 (3)					
free	0			2.82 (±0.06)	$\leq 1 \times 10^4$
MPIX	0			2.89 (±0.02)	$\leq 1 \times 10^4$
B: 384–394 (10)					
free	~1.9	4.4 (±0.8)	2.6 (±0.6)	3.7 (±0.5)	0.08 (±0.02)
MPIX	~2.4	3.7 (±0.8)	0.97 (±0.07)	3.9 (±0.8)	0.06 (±0.03)
C: 195–203 (8)					
free	0			5.7 (±0.1)	$6.2 (\pm 0.8) \times 10^3$
MPIX	~3			3.05 (±0.07)	$\leq 1 \times 10^4$

[a]Parameters obtained from fitting the H/D-exchange kinetics of ferrochelatase peptides with and without MPIX (Figure 4 B–D) according to a single or double exponential expression. The number in parentheses is the total possible number of exchangeable amide hydrogens (N) for that peptide. The rates have been loosely grouped in to fast, intermediate, and slow exchange. [b]The amount of exchange before the first time point (15 s) is estimated from the fit parameters and is assigned a rate of exchange > 4 min^{-1}. [c]The amount of deuterium in the slowest phase was determined $D_2 = N - D_1 - D_{\text{pre-exchanged}}$.

backbone alterations in the PPIX structure.[20] In total, MPIX-based solvent accessibility changes in the upper lip are localized to α-helices 1 and 2. Given that the upper lip inserts into the inner mitochondrial membrane, it is tempting to speculate that conformational and solubility changes in this region may be linked to acquisition of PPIX from protoporphyrinogen oxidase, the integral membrane enzyme upstream of ferrochelatase in the heme biosynthetic pathway with which ferrochelatase is postulated to interact.[35,36] We hypothesize that once the porphyrin is metalated, that these peptides should have HDX kinetics similar to the free enzyme so that the mouth opens and product is released.

N-terminal to the upper lip, but still within interaction distance with PPIX, is peptide 74–89 (Figure 4A, purple). Peptide 74–89 is a loop that ends within $helix_1$ and contains M76 whose side chain is directly above the porphyrin pyrrole nitrogens of human ferrochelatase (Figure 5B).[12] M76 is a catalytically essential residue whose mutation has complete loss of ferrochelatase activity.[17] This region has a small change in initial solvent accessibility and reduced backbone dynamics with MPIX that lead to less overall deuterium incorporation compared to free-enzyme. This result is consistent with small backbone differences in the aligned ferrochelatase structures[20] (Figure 4). Also, this peptide does not change conformation with iron;[19] therefore, the backbone dynamic constraints imposed on the loop are only from interaction with MPIX. In terms of function, M76 may help insert iron into the macrocycle or stabilize the metalated product,[31] and thus prestabilization of the backbone surrounding this key residue before PPIX binding could be highly relevant for catalytic efficiency, especially if M76 is directly involved in metalation. Only eukaryotic ferrochelatases have this conserved residue; therefore, the stabilization we observe might not be applicable to other ferrochelatase enzymes.[31]

Now that contributions from the upper lip have been dissected, we can compare those to the lower lip (residues 300–311), which is a 12 amino acid loop linking β-$strand_6$ and $helix_{12}$. As expected for a loop, amide hydrogens from peptide 303–317 are readily exchanged for deuterons with similar rates in both free- and MPIX-bound ferrochelatase (Figure 3D) despite the numerous side chain contacts to PPIX such as V305 and W310 (Figure 5C). The high amount of exchange in the loop is driven by the presence of D_2O in the pocket and the lack of amide hydrogen bonds. The slight decrease in overall deuterium content with MPIX-ferrochelatase could be from partial exclusion of solvent when the active site mouth closes around the porphyrin substrate or from amide protection by bonding. Consistent with HDX results, the backbone deviation

dx.doi.org/10.1021/bi300704c | *Biochemistry* 2012, 51, 7116–7127

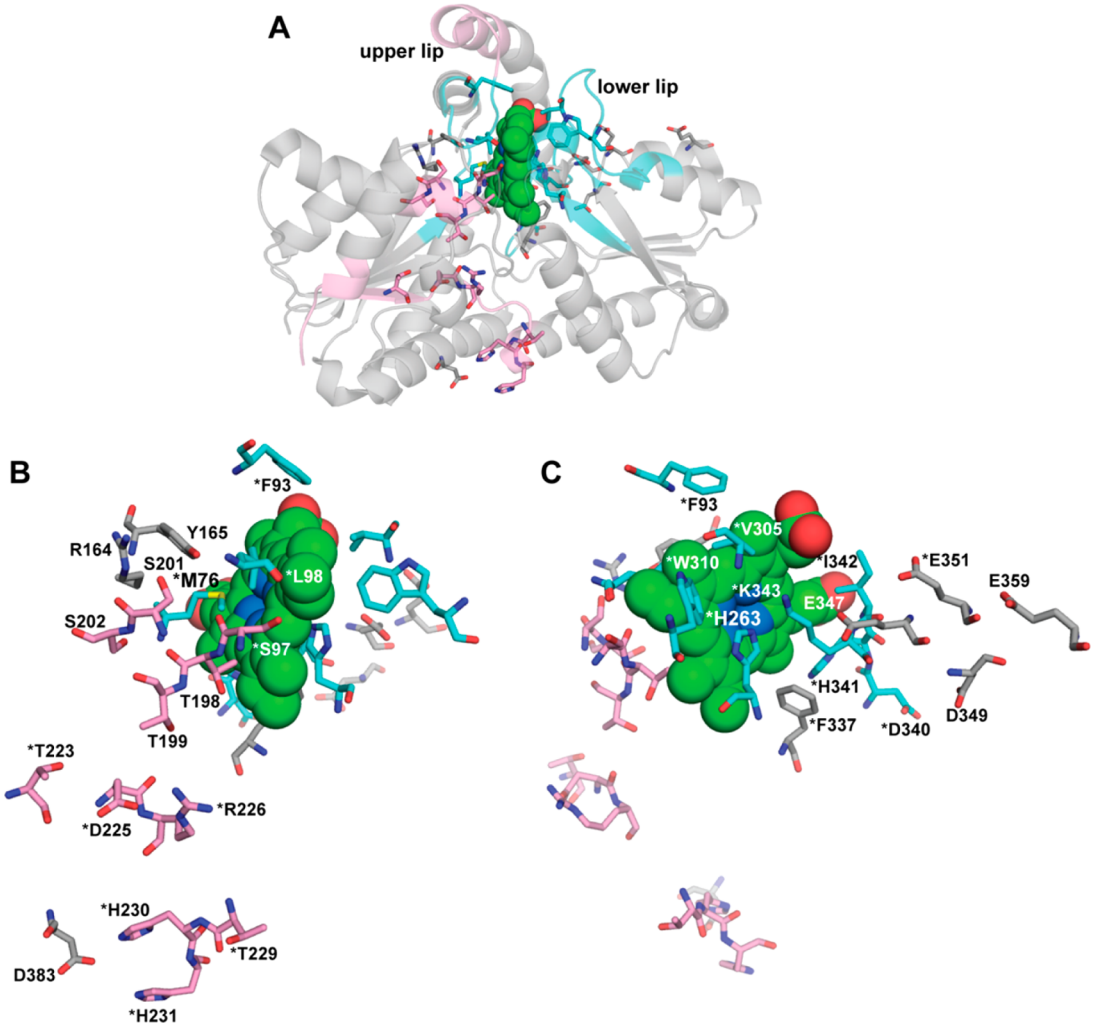

Figure 5. MPIX-bound ferrochelatase solvent accessibility structural maps. (A) Peptides that have increased (pink) or decreased (cyan) D_2O accessibility from HDX-MS are mapped to the monomeric ferrochelatase structure with PPIX bound (green spheres).[20] Data were taken from Figure 1. (B) Residues with increased deuterium access cluster on one face of the porphyrin and several key residues that could be involved in an iron channel are indicated in stick format. Residues with an asterisk (*) are from peptides that have decreased backbone dynamics in the presence of MPIX (Figure 3). (C) Residues with decreased deuterium access cluster on the lower lip side of the porphyrin (Figure 3). Key residues that could be involved in an iron channel are indicated in stick format. Residues with an asterisk (*) are from peptides that have decreased backbone dynamics in the presence of MPIX. Figure created with PyMOL.[32]

within residues 303−317 of the free and PPIX aligned structures is small but there is a noticeable shift closer to the porphyrin[20] (Figure 4, cyan). HDX with Fe^{2+}-ferrochelatase has a similar kinetic profile to the free enzyme;[19] therefore, we can assume the dynamic change in the lower lip is specific for porphyrin. Residues within 303−317 must be important to the catalytic mechanism or structure of ferrochelatase since five are fully conserved and three are highly conserved among eukaryotic and prokaryotic ferrochelatases.[31] Random mutagenesis of the murine ferrochelatase lower lip (human numbering 320−311) indicated that most substitutions increase the K_m for PPIX and that residues S303, G306, W310, and L311 were intolerant to most mutations.[37] We propose that the lower lip is dynamically constrained even in the *absence* of porphyrin substrate and that porphyrin access to the active site is controlled only by reorientation of the upper lip to open and close the pocket. It is interesting that ferrochelatase preorients and stabilizes the lower lip in the free enzyme. A lack of dynamics would lead to efficient substrate binding and/or porphyrin substrate orientation. Medlock and co-workers suggested that the interactions between PPIX and hydrophobic residues within 303−317 could be the trigger for closure of the upper lip.[12] Our HDX-MS results are consistent with that hypothesis, where porphyrin binding does not require substantial conformational change in the lower lip and is thus is not rate-limiting.

Residues Surrounding the Porphyrin Pocket Mediate the Conformational Response. Turning to the bottom of the porphyrin binding pocket, we observed two adjacent peptides that have a conformational response to MPIX, peptides 332−337 and 338−345. In free-ferrochelatase, peptide 332−337 incorporates ∼50% deuterium over 2 h indicating moderate solvent accessibility and backbone dynamics in the absence of substrate (Figure 3F). When MPIX binds, the backbone dynamics are completely abrogated despite the small increase in D_2O access within the first 15 s of deuteration. The loss of backbone dynamics is probably due an interaction between F337 and porphyrin. Consistent with this, the F337A mutation increases the K_m for PPIX about 2-fold.[17] The structures of ferrochelatase clearly show the F337 benzyl ring in

dx.doi.org/10.1021/bi300704c | *Biochemistry* 2012, 51, 7116−7127

different positions with and without PPIX, but with little change in the backbone orientation[20] (Figure 4, blue). It has been postulated that the benzyl ring of F337 is a gate between solvent channels to and from the active site. HDX-MS suggests that the conformation of the backbone is significantly less dynamic if MPIX is bound. If the backbone is more dynamic in the free enzyme, MPIX binding to F337 would restrict its motion, allowing the side chain to change conformation to control access of iron via a solvent channel to the active site. Thus the F337 interaction could be the sensor for porphyrin binding site that triggers the iron uptake conformation. Residues 332−337 do not have a conformational response to Fe^{2+}, which lends more support for a functional role with PPIX.[19]

Adjacent to 332−337 is the π-helix$_{13}$ peptide 338−345 that responds to MPIX binding with a striking decrease in backbone deuterium access (Figure 3G). Several residue side chains are within interaction distance to the porphyrin including H341 and I342, and there is a high level of amino acid conservation across all ferrochelatases, especially for E343[16] (Figure 5C). Mutations of D340 and E343 revealed that the acidic side chains of these residues are required for activity.[17,31] Unlike MPIX, Fe^{2+} binding to free-ferrochelatase does not lead to changes in solvent accessibility for peptide 338−345.[19] Thus, this particular region is probably not involved in "sensing" iron, but instead MPIX through interaction with specific residues like E343. Another π-helix$_{13}$ peptide, 350−356, is farther down the π-helix$_{13}$ and has no change in solvent accessibility but has a slight decrease in dynamics (Figure 3J). Thus, only the residues at the *N*-terminal end of the π-helix$_{13}$ are critical for binding MPIX and for the functional conformational response by constraining dynamics that might facilitate premature release of substrate instead of product.

Localization of Porphyrin and Iron Responsive Regions Gives Insight into the Ferrochelatase Mechanism. It is generally agreed that ferrochelatase has an ordered mechanism where PPIX binds first, followed by iron binding and insertion into the macrocycle.[38] The exact entrance route taken by iron would greatly clarify the mechanism of ferrochelatase since it could dictate from which face of the porphyrin it is inserted. We hypothesize that MPIX binding should be structurally linked to Fe^{2+} uptake, so we examined regions that had higher solvent accessibility with MPIX bound. The rationale is that there must be a channel or path that the Fe^{2+} takes to the active site and that channel must open in response to porphyrin substrate binding. There should also be a decrease in backbone dynamics to stabilize the channel and the channel should become more restrictive to solvent closer to the active site once hydrating waters are removed from the iron.[39] Figure 5 shows peptides with a change in D_2O accessibility and the specific residues that might be important to the structure and mechanism of ferrochelatase. It is clear that peptides with increased deuterium incorporation from solvent effects are clustered on one side of the porphyrin and lead to the surface of the enzyme (Figure 5A, pink). This is consistent with a conformational response after MPIX binding that links the active site to a solvent accessible channel.

We then compared the HDX results for MPIX and Fe^{2+} to identify peptides that have a similar response to both substrates. There were four choices: peptides 99−112 in the upper lip, 332−337 at the bottom of the active site, 222−233 at the surface facing the matrix, and 195−203 that bridges the active site and the [2Fe-2S] cluster. The upper lip peptide was ruled out since there is no direct evidence that iron would be inserted from the membrane side of ferrochelatase. A recent report demonstrated that the mitochondrial iron importer mitoferrin forms a complex with ferrochelatase and it is proposed that mitoferrin could deliver iron through the membrane.[40] Peptide 332−337 has a very small increase in solvent accessibility and is buried so this peptide was not considered further, at least for the entrance of iron. It is possible that residues 332−337 are a part of the iron channel, but since it is much closer to PPIX it could be more solvent restricted than other regions. This leaves peptides 222−233 and 195−203 as potential candidates for lining the solvent filled iron channel.

Peptide 222−233 is located on the surface of ferrochelatase and contains a few potential metal binding residues like D225, H230, and H231 (Figure 5B). It has a significant increase in solvent accessibility and decrease in backbone dynamics over the times measured when MPIX binds (Figure 3H). As with peptide 99−112, it is also possible that conformational changes with MPIX resulting in increased deuterium incorporation could occur before our first time point (15 s), but after which no more deuterium is incorporated. Therefore, we are comparing the much slower motions in this region with our analysis. An alignment of the free- and PPIX-bound structures does not reveal backbone deviation in this region (Figure 4, pink), but HDX shows a dynamic response to MPIX. Interestingly, the HDX rate profile with MIPX bound is indistinguishable from that with Fe^{2+} bound;[19] thus, porphyrin substrate binding results in a similar conformational change as Fe^{2+} binding. This structural link to *both* substrates is a good indication of an iron channel peptide. Combining the HDX results for MPIX with that for Fe^{2+}, we hypothesize that residues within 222−233 respond to MPIX binding to open the iron channel for efficient iron entry, thus exposing more backbone amides to solvent. Previous crystal structures observed that Co^{2+} can coordinate the imidazole side chain of H231 along with the carboxylate side chain of D383.[8] It has been proposed that Fe^{2+} initially binds to H231 and D383 before it is channeled to the postulated terminal ligands, R164 and Y165, for insertion into the porphyrin macrocycle[31] (Figure 5B). Unfortunately a peptide that includes D383 was not identified, but peptide 384−394 (Figure 4, salmon) is fairly solvent accessible and dynamic in both free- and MPIX-ferrochelatase (Figure 4C). Like peptide 222−233, this peptide has a small decrease in backbone flexibility with both MPIX and iron, again structurally linking this region to both substrates. The conformational link between MPIX and an iron channel may explain why mutation of H231 to alanine, which is over 20 Å away from the active site, increases the K_m for Fe^{2+} but not for MPIX. Other mutations like W227Y and D383A in this region also increase the K_m for iron.[31] It is tempting to speculate that the H231A mutation may abrogate the Fe^{2+} and MPIX conformational response observed by HDX. There are some reports that suggest that Fe^{2+} is delivered to ferrochelatase by the iron chaperone frataxin.[41,42] A recent docking model showed that two aspartate residues of frataxin could be placed within 9 Å of H231 and D383 of ferrochelatase.[41] Thus, the change in conformation for ferrochelatase around surface residues 222−233 could also be required for efficient interaction with frataxin, but there is no direct evidence that the interaction occurs *in vivo*.

The other ferrochelatase peptide meeting the criteria of a channel is 195−203 whose backbone amides are more accessible to D_2O in both the MPIX (Figure 4D) and iron

bound forms.[19] This peptide spans the region between PPIX and the [2Fe-2S] cluster (Figure 4, dark teal). Side chain and backbone atoms within peptide 195−203 (T198, S200, S201) participate in multiple hydrogen bonding interactions with surrounding residues in the free-enzyme that rearrange in the PPIX-bound structure without significant changes in backbone conformation[20] (Figure 4A). However, HDX with the Fe^{2+}-bound enzyme indicates that peptide 195−203 has more conformational flexibility than in the free- and MPIX states. This would imply that interactions with PPIX are needed to stabilize conformation and control iron insertion into the porphyrin. It also suggests that past this region, there should be solvent restriction to ensure that dehydrated iron is bound at the terminal acceptors before insertion in the PPIX macrocycle.

The alternate hypothesis delivers Fe^{2+} to the terminal ligands H263 and E343 via an anionic surface on the π-helix$_{13}$[10,43] (Figure 5C). H263 would then serve as the metal donor residue for insertion into PPIX. Visual inspection of the solvent accessibility of amides on this face of the porphyrin ring shows a general decrease around the MPIX binding site, with no large increases in deuteration (Figure 5C). Peptides that span the π-helix$_{13}$ include 338−345 and 350−356 and both regions have decreased dynamics when MPIX is bound (Figure 3G,J). Thus, the dynamic alterations we observe with MPIX were not apparent in the crystal structure (Figure 4, orange and yellow). Also the HDX kinetics for both π-helix$_{13}$ peptides do not change substantially with Fe^{2+} present,[19] which is curious if this was the channel for iron. These results are consistent with a role in porphyrin substrate binding. Mutagenesis of π-helix$_{13}$ residues D340E, E343D, and H341C reduced activity without a significant change in K_m for either Fe^{2+} or PPIX, which should be expected if they are involved in channeling iron to the active site.[31] Also since this face of the active site pocket is relatively inaccessible to solvent with MPIX present, nonspecific channeling of hydrated iron is also unlikely.[17] If H263 is the terminal acceptor of iron before insertion in to PPIX, the solvent accessibility of peptide 260−269 should be decreased so that the iron is dehydrated properly and the dynamics should be reduced in the MPIX bound state. This is, in fact, what is observed from HDX (Figure 3E). The other possibility is that D340, E343, and E347 may be involved in abstraction of protons from the pyrrole nitrogens prior to metalation,[31,44] which would occur via the opposite face of the macrocycle as H263.[20] This too would require a stable surface. Since H263 is a critical residue for ferrochelatase activity, the preorganization of residues within 260−269 must be essential for its catalytic function, whether iron insertion or pyrrole extraction.

CONCLUSIONS

HDX-MS indicates that porphyrin binding to ferrochelatase signals dynamic changes in regions inside and outside the vicinity of the active site without large changes in the structure. When comparing the free- and PPIX-ferrochelatase aligned crystal structures,[20] the largest changes in conformation were also verified by H/D exchange behavior of peptides in these regions. However, new and potentially important dynamic regions of ferrochelatase have been identified by HDX-MS that warrant further structure−function investigation. These areas have not been functionally characterized as extensively as the regions around the active site, but they are clearly important structural contributors to the catalytic mechanism. Through comparison with previous HDX-MS experiments localizing the structural response to iron substrate binding, insight into the coupling of PPIX binding with Fe^{2+} uptake was illuminated, thus providing a more detailed conformational view of the ferrochelatase mechanism. HDX-MS clearly shows that regions previously identified as responsive to iron also behave similarly to porphyrin, and thus we have structurally linked iron and porphyrin binding for the first time. We propose that porphyrin substrate binding is propagated via conformational and dynamic changes that ultimately open a channel for iron uptake at the matrix-facing side of ferrochelatase, while stabilizing the active site pocket where the porphyrin in bound. While HDX-MS cannot rule one pathway in or out for metal uptake and insertion, the results presented here provide more support to the highly debated mechanism whereby iron is inserted into PPIX from the M76/R164/Y165 side of the macrocycle.

ASSOCIATED CONTENT

Supporting Information

The pepsin digest peptide map of ferrochelatase (Figure S1) and all HDX-MS progress curves with fits for each peptide (Figure S2) are provided. This material is available free of charge via the Internet at http://pubs.acs.org.

AUTHOR INFORMATION

Corresponding Author

*Phone, 205-348-0269. Fax, 205-348-9104. E-mail, LSBusenlehner@bama.ua.edu.

Funding

This work was supported by the National Science Foundation Award No. 0845273 (to L.S.B.) and by the Ronald E. McNair Post-Baccalaureate Achievement Program (McNair Scholars) of The University of Alabama, U.S. Department of Education TRIO Grant P217A030031 (to A.P.A.). The National Science Foundation CRIF program (CHE 0639003) is acknowledged for purchase of the mass spectrometer used in this study.

Notes

The authors declare no competing financial interest.

ACKNOWLEDGMENTS

The authors would like to thank the Department of Chemistry Mass Spectrometry Resource Facility manager, Dr. Qiaoli Liang, for help with instrumentation and Dr. Harry Dailey (University of Georgia) for his gift of the ferrochelatase plasmid.

ABBREVIATIONS USED

HDX-MS, hydrogen/deuterium exchange mass spectrometry; β-ME, 2-mercaptoethanol; CHAPS, 3-[(3-cholamidopropyl)-dimethylammonio]-2-hydroxy-1-propanesulfonate; MPIX, mesoporphyrin IX; PPIX, protoporphyrin IX; D_2O, deuterium oxide

REFERENCES

(1) Busenlehner, L. S., and Armstrong, R. N. (2005) Insights into enzyme structure and dynamics elucidated by amide H/D exchange mass spectrometry. *Arch. Biochem. Biophys. 433*, 34−46.

(2) Eisenmesser, E. Z., Millet, O., Labeikovsky, W., Korzhnev, D. M., Wolf-Watz, M., Bosco, D. A., Skalicky, J. J., Kay, L. E., and Kern, D. (2005) Intrinsic dynamics of an enzyme underlies catalysis. *Nature 438*, 117−121.

(3) Schramm, V. L. (2011) Enzymatic transition states, transition-state analogs, dynamics, thermodynamics, and lifetimes. *Annu. Rev. Biochem. 80*, 703−732.

(4) Bakan, A., and Bahar, I. (2009) The intrinsic dynamics of enzymes plays a dominant role in determining the structural changes induced upon inhibitor binding. *Proc. Natl. Acad. Sci. U.S.A. 106*, 14349−14354.
(5) Dailey, H. A., Dailey, T. A. (2003) Ferrochelatase, in *The Porphyrin Handbook* (Kadish, K. M., Smith, K. M., Guilard, R., Eds.) pp 93−121, Elsevier Science.
(6) Sellers, V. M., Dailey, T. A., and Dailey, H. A. (1998) Examination of ferrochelatase mutations that cause erythropoietic protoporphyria. *Blood 91*, 3980−3985.
(7) Taketani, S., and Fujita, H. (1995) The ferrochelatase gene structure and molecular defects associated with erythropoietic protoporphyria. *J. Bioenerg. Biomembr. 27*, 231−238.
(8) Wu, C. K., Dailey, H. A., Rose, J. P., Burden, A., Sellers, V. M., and Wang, B. C. (2001) The 2.0 Å structure of human ferrochelatase, the terminal enzyme of heme biosynthesis. *Nat. Struct. Biol. 8*, 156−160.
(9) Burden, A. E., Wu, C., Dailey, T. A., Busch, J. L., Dhawan, I. K., Rose, J. P., Wang, B., and Dailey, H. A. (1999) Human ferrochelatase: Crystallization, characterization of the [2Fe-2S] cluster and determination that the enzyme is a homodimer. *Biochim. Biophys. Acta 1435*, 191−197.
(10) Karlberg, T., Lecerof, D., Gora, M., Silvegren, G., Labbe-Bois, R., Hansson, M., and Al-Karadaghi, S. (2002) Metal binding to *Saccharomyces cerevisiae* ferrochelatase. *Biochemistry 41*, 13499−13506.
(11) Al-Karadaghi, S., Hansson, M., Nikonov, S., Jonsson, B., and Hederstedt, L. (1997) Crystal structure of ferrochelatase: The terminal enzyme in heme biosynthesis. *Structure 5*, 1501−1510.
(12) Medlock, A., Swartz, L., Dailey, T. A., Dailey, H. A., and Lanzilotta, W. N. (2007) Substrate interactions with human ferrochelatase. *Proc. Natl. Acad. Sci. U. S. A. 104*, 1789−1793.
(13) Medlock, A. E., Carter, M., Dailey, T. A., Dailey, H. A., and Lanzilotta, W. N. (2009) Product release rather than chelation determines metal specificity for ferrochelatase. *J. Mol. Biol. 393*, 308−319.
(14) Karlberg, T., Hansson, M. D., Yengo, R. K., Johansson, R., Thorvaldsen, H. O., Ferreira, G. C., Hansson, M., and Al-Karadaghi, S. (2008) Porphyrin binding and distortion and substrate specificity in the ferrochelatase reaction: The role of active site residues. *J. Mol. Biol. 378*, 1074−1083.
(15) Lecerof, D., Fodje, M., Hansson, A., Hansson, M., and Al-Karadaghi, S. (2000) Structural and mechanistic basis of porphyrin metallation by ferrochelatase. *J. Mol. Biol. 297*, 221−232.
(16) Dailey, H. A., Dailey, T. A., Wu, C. K., Medlock, A. E., Wang, K. F., Rose, J. P., and Wang, B. C. (2000) Ferrochelatase at the millennium: Structures, mechanisms and [2Fe-2S] clusters. *Cell. Mol. Life Sci. 57*, 1909−1926.
(17) Dailey, H. A., Wu, C. K., Horanyi, P., Medlock, A. E., Najahi-Missaoui, W., Burden, A. E., Dailey, T. A., and Rose, J. (2007) Altered orientation of active site residues in variants of human ferrochelatase. Evidence for a hydrogen bond network involved in catalysis. *Biochemistry 46*, 7973−7979.
(18) Hunter, G. A., Al-Karadaghi, S., and Ferreira, G. C. (2011) Ferrochelatase: The convergence of the porphyrin biosynthesis and iron transport pathways. *J. Porphyr. Phthalocyanines 15*, 350−356.
(19) Asuru, A. P., and Busenlehner, L. S. (2011) Analysis of human ferrochelatase iron binding via amide hydrogen/deuterium exchange mass spectrometry. *Intl. J. Mass Spectrom. 302*, 76−84.
(20) Medlock, A. E., Dailey, T. A., Ross, T. A., Dailey, H. A., and Lanzilotta, W. N. (2007) A pi-helix switch selective for porphyrin deprotonation and product release in human ferrochelatase. *J. Mol. Biol. 373*, 1006−1016.
(21) Okuda, M., Kohno, H., Furukawa, T., Tokunaga, R., and Taketani, S. (1994) Overexpression in *Escherichia coli*, and one-step purification of the human recombinant ferrochelatase. *Biochim. Biophys. Acta 1200*, 123−128.
(22) Dailey, H. A. (2002) Terminal steps of haem biosynthesis. *Biochem. Soc. Trans. 30*, 590−595.
(23) Zhang, Z., and Marshall, A. G. (1998) A universal algorithm for fast and automated charge state deconvolution of electrospray mass-to-charge ratio spectra. *J. Am. Soc. Mass Spectrom. 9*, 225−233.
(24) Zhang, Z., and Smith, D. L. (1993) Determination of amide hydrogen exchange by mass spectrometry: A new tool for protein structure elucidation. *Protein Sci. 2*, 522−531.
(25) Bai, Y., Milne, J. S., Mayne, L., and Englander, S. W. (1993) Primary structure effects on peptide group hydrogen exchange. *Proteins 17*, 75−86.
(26) Molday, R. S., Englander, S. W., and Kallen, R. G. (1972) Primary structure effects on peptide group hydrogen exchange. *Biochemistry 11*, 150−158.
(27) Dharmasiri, K., and Smith, D. L. (1996) Mass spectrometric determination of isotopic exchange rates of amide hydrogens located on the surfaces of proteins. *Anal. Chem. 68*, 2340−2344.
(28) Smith, D. L., Deng, Y., and Zhang, Z. (1997) Probing the non-covalent structure of proteins by amide hydrogen exchange and mass spectrometry. *J. Mass Spectrom. 32*, 135−146.
(29) Mandell, J. G., Baerga-Ortiz, A., Croy, C. H., Falick, A. M., Komives, E. A. (2005) Application of amide proton exchange mass spectrometry for the study of protein-protein interactions. *Curr. Protoc. Protein Sci.* Chapter 20, Unit 20.9.
(30) Busenlehner, L. S., Alander, J., Jegerscohld, C., Holm, P. J., Bhakat, P., Hebert, H., Morgenstern, R., and Armstrong, R. N. (2007) Location of substrate binding sites within the integral membrane protein microsomal glutathione transferase-1. *Biochemistry 46*, 2812−2822.
(31) Sellers, V. M., Wu, C. K., Dailey, T. A., and Dailey, H. A. (2001) Human ferrochelatase: Characterization of substrate-iron binding and proton-abstracting residues. *Biochemistry 40*, 9821−9827.
(32) Schrodinger, L. L. C. (2010) The PyMol molecular graphics system, version 1.3r1.
(33) Engen, J. R., and Smith, D. L. (2001) Investigating protein structure and dynamics by hydrogen exchange MS. *Anal. Chem. 73*, 256A−265A.
(34) Chalmers, M. J., Busby, S. A., Pascal, B. D., West, G. M., and Griffin, P. R. (2011) Differential hydrogen/deuterium exchange mass spectrometry analysis of protein-ligand interactions. *Expert Rev. Proteomics 8*, 43−59.
(35) Ajioka, R. S., Phillips, J. D., and Kushner, J. P. (2006) Biosynthesis of heme in mammals. *Biochim. Biophys. Acta 1763*, 723−736.
(36) Masoumi, A., Heinemann, I. U., Rohde, M., Koch, M., Jahn, M., and Jahn, D. (2008) Complex formation between protoporphyrinogen IX oxidase and ferrochelatase during haem biosynthesis in *Thermosynechococcus elongatus*. *Microbiology 154*, 3707−3714.
(37) Shi, Z., and Ferreira, G. C. (2004) Probing the active site loop motif of murine ferrochelatase by random mutagenesis. *J. Biol. Chem. 279*, 19977−19986.
(38) Davidson, R. E., Chesters, C. J., and Reid, J. D. (2009) Metal ion selectivity and substrate inhibition in the metal ion chelation catalyzed by human ferrochelatase. *J. Biol. Chem. 284*, 33795−33799.
(39) Banci, L., Bertini, I., Cantini, F., D'Onofrio, M., and Viezzoli, M. S. (2002) Structure and dynamics of copper-free sod: The protein before binding copper. *Protein Sci. 11*, 2479−2492.
(40) Chen, W., Dailey, H. A., and Paw, B. H. (2010) Ferrochelatase forms an oligomeric complex with mitoferrin-1 and abcb10 for erythroid heme biosynthesis. *Blood 116*, 628−630.
(41) Bencze, K. Z., Yoon, T., Millan-Pacheco, C., Bradley, P. B., Pastor, N., Cowan, J. A., and Stemmler, T. L. (2007) Human frataxin: Iron and ferrochelatase binding surface. *Chem. Commun. (Camb)*, 1798−1800.
(42) Yoon, T., and Cowan, J. A. (2004) Frataxin-mediated iron delivery to ferrochelatase in the final step of heme biosynthesis. *J. Biol. Chem. 279*, 25943−25946.
(43) Hansson, M. D., Karlberg, T., Rahardja, M. A., Al-Karadaghi, S., and Hansson, M. (2007) Amino acid residues His183 and Glu264 in *Bacillus subtilis* ferrochelatase direct and facilitate the insertion of metal ion into protoporphyrin ix. *Biochemistry 46*, 87−94.

(44) Gora, M., Grzybowska, E., Rytka, J., and Labbe-Bois, R. (1996) Probing the active-site residues in *Saccharomyces cerevisiae* ferrochelatase by directed mutagenesis. *In vivo* and *in vitro* analyses. *J. Biol. Chem. 271,* 11810−11816.